Colloidal hard-rod fluids near geometrically structured substrates

L. Harnau,[1,2] F. Penna,[3] and S. Dietrich[1,2]
[1]*Max-Planck-Institut für Metallforschung, Heisenbergstr. 3, D-70569 Stuttgart, Germany*
[2]*Institut für Theoretische und Angewandte Physik, Universität Stuttgart, Pfaffenwaldring 57, D-70569 Stuttgart, Germany*
[3]*Departamento de Fisica Teórica de la Materia Condensada, Universidad Autónoma de Madrid, E-28049 Madrid, Spain*
(Received 29 March 2004; published 13 August 2004)

Density functional theory is used to study colloidal hard-rod fluids near an individual right-angled wedge or edge as well as near a hard wall, which is periodically patterned with rectangular barriers. The Zwanzig model, in which the orientations of the rods are restricted to three orthogonal orientations but their positions can vary continuously, is analyzed by numerical minimization of the grand potential. Density and orientational order profiles, excess adsorptions, as well as surface and line tensions are determined. The calculations exhibit an enrichment [depletion] of rods lying parallel and close to the corner of the wedge (edge). For the fluid near the geometrically patterned wall, complete wetting of the wall—isotropic liquid interface by a nematic film occurs as a two-stage process in which first the nematic phase fills the space between the barriers until an almost planar isotropic—nematic liquid interface has formed separating the higher-density nematic fluid in the space between the barriers from the lower-density isotropic bulk fluid. In the second stage, a nematic film of diverging film thickness develops upon approaching bulk-isotropic–nematic coexistence.

DOI: 10.1103/PhysRevE.70.021505 PACS number(s): 61.20.−p, 61.30.Gd, 82.70.Dd

I. INTRODUCTION

There is growing interest in properties of suspensions of colloidal particles near structured walls because of useful applications, such as selective deposition of particles [1] and controlled growth of colloidal crystals [2]. While experimental [1,2], theoretical [3–6], and computer simulation [7–10] studies have been devoted to the understanding of the behavior of spherical colloidal particles near geometrically structured substrates, suspensions of rodlike colloidal particles in contact with such substrates have not been investigated yet, despite the importance of rodlike colloids for both biological and materials application. From a theoretical point of view, as compared with fluids consisting of spherical particles, the study of rods is more difficult because of the additional orientational degrees of freedom.

Here we study hard-rod fluids near geometrically structured walls within the Zwanzig approximation [11]. In this model the allowed orientations of the rods are restricted to three mutually perpendicular orientations rather than a continuous range of orientations in space (see Fig. 1); the positions of the rod centers are continuous variables. The advantage of this model is that the difficult determination of spatially inhomogeneous density and orientational order profiles becomes feasible allowing one to study various aspects of hard-rod fluids near structured walls in detail. On the basis of recent theoretical studies on fluids of hard rods near planar hard walls [12–14], we expect to find results that remain qualitatively correct even in the absence of the restriction to discrete orientational directions. In Sec. II we describe the density functional theory, which is used to analyze a hard-rod fluid in contact with an individual right-angled wedge or edge (Sec. III) or with a periodically patterned wall (Sec. IV).

II. MODEL AND DENSITY FUNCTIONAL THEORY

We consider an inhomogeneous fluid consisting of hard rods of length L and thickness $D \ll L$. The number density of the centers of mass of the rods at point $\mathbf{r}$ with orientation $\omega=(\theta,\phi)$ of the normal along their main axis of symmetry is denoted as $\rho(\mathbf{r},\omega)$. The equilibrium density profile of the inhomogeneous liquid under the influence of an external field $V_{ext}(\mathbf{r},\omega)$ minimizes the grand potential functional

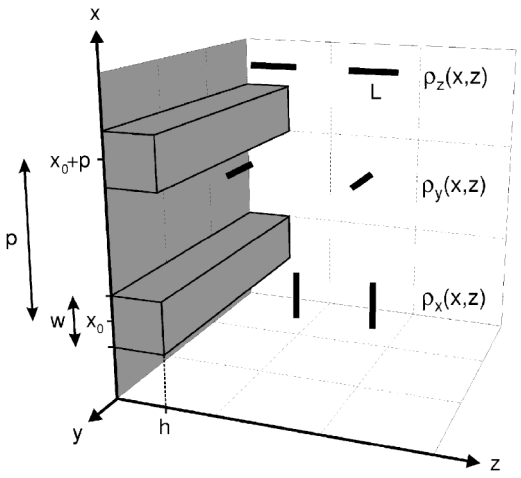

FIG. 1. The system under consideration consists of a fluid of thin hard rods of length L and thickness $D \ll L$ in contact with a hard substrate (gray). The surface $z_s(x)$ of the substrate wall exhibits a periodic pattern with period p consisting of rectangular blocks of width w and height h. The density profiles for the centers of the rods with an orientation of the normal along their main axis of symmetry parallel to the orthogonal unit vectors of the reference frame are denoted as $\rho_x(x,z)$, $\rho_y(x,z)$, and $\rho_z(x,z)$. The system is spatially invariant in the y direction. In accordance with the discreteness of the orientational degrees of freedom $\rho_z[x,z<z_s(x)+L/2]=0$, $\rho_x[x_0+np-(w+L)/2<x<x_0+np+(w+L)/2,z<h]=0$ with $n\in\mathbb{Z}$, and $\rho_{x,y}[x,z<z_s(x)]=0$ where $z_s(x_0+np-w/2<x<x_0+np+w/2)=h$ and $z_s(x)=0$ otherwise. The value of x_0 is arbitrary.

$$\Omega[\rho(\mathbf{r},\omega)] = \int d^3r d\omega \rho(\mathbf{r},\omega)[k_BT(\ln[4\pi\Lambda^3\rho(\mathbf{r},\omega)] - 1) - \mu + V_{ext}(\mathbf{r},\omega)] + F_{ex}[\rho(\mathbf{r},\omega)], \quad (1)$$

where Λ is the thermal de Broglie wavelength and μ is the chemical potential. Within the Onsager second virial approximation, the free-energy functional $F_{ex}[\rho(\mathbf{r},\omega)]$ in excess of the ideal gas contribution reads [15]

$$F_{ex}[\rho(\mathbf{r},\omega)] = -\frac{k_BT}{2}\int d^3r_1 d\omega_1 d^3r_2 d\omega_2 \rho(\mathbf{r}_1,\omega_1)\rho(\mathbf{r}_2,\omega_2) \times f(\mathbf{r}_1,\mathbf{r}_2,\omega_1,\omega_2), \quad (2)$$

where $f(\mathbf{r}_1,\mathbf{r}_2,\omega_1,\omega_2)$ is the Mayer function of the interaction potential between two rods. The Mayer function equals -1 if the rods overlap and is zero otherwise. Onsager demonstrated that the second virial approximation becomes exact in the limit of thin needlelike rods ($D \ll L$) for the bulk fluid because of the infinitesimal probability that three or more rods will simultaneously intersect [15].

In the present application of density functional theory, we concentrate on the ordering effects induced by surfaces geometrically structured such that the resulting $\rho(\mathbf{r},\omega)$ depends on two spatial coordinates. For the model system displayed in Fig. 1, apart from the possibility of surface freezing at high densities, nonuniformities of the density occur only in the x-z plane, so that $\rho(\mathbf{r},\omega)=\rho(x,z,\theta,\phi)$. Minimization of Ω with respect to $\rho(x,z,\theta,\phi)$ leads to the following Euler-Langrange equation:

$$k_BT\ln[4\pi\Lambda^3\rho(x,z,\theta,\phi)] = \mu - V_{ext}(x,z,\theta,\phi) + \int dx_1 dy_1 dz_1 \int_0^{2\pi} d\phi_1 \int_0^{\pi} d\theta_1 \sin\theta_1 \times \rho(x_1,z_1,\theta_1,\phi_1) f(x,z,\theta,\phi,x_1,y_1,z_1,\theta_1,\phi_1) k_BT. \quad (3)$$

This equation can be solved numerically for a given chemical potential μ and a given external field $V(x,z,\theta,\phi)$. For computational purposes, the density profile has to be specified on a sufficiently fine 4D (x,z,θ,ϕ) grid. In order to reduce this computational effort we use the Zwanzig model for rods [11]. Within the Zwanzig model the rods are represented by rectangular blocks of size $L\times D\times D$. The positions of the center of mass vary continuously, while the allowed orientations of the normal of each rod are restricted to directions parallel to the x, y, and z axis (see Fig. 1). Using the notation $\alpha_x(x,z)=\alpha(x,z,\theta=\pi/2,\phi=0)$, $\alpha_y(x,z)=\alpha(x,z,\theta=\pi/2,\phi=\pi/2)$, and $\alpha_z(x,z)=\alpha(x,z,\theta=0,\phi=0)$ with $\alpha=\rho, V_{ext}$, the Euler-Lagrange equations for a fluid consisting of thin Zwanzig rods can be written as

$$\ln[\Lambda^3\rho_x(x,z)] = (k_BT)^{-1}[\mu - V_{ext,x}(x,z)] - 2DL\int_{x-L/2}^{x+L/2} dx_1 \rho_y(x_1,z) - 2D\int_{x-L/2}^{x+L/2} dx_1 \int_{z-L/2}^{z+L/2} dz_1 \rho_z(x_1,z_1), \quad (4)$$

$$\ln[\Lambda^3\rho_y(x,z)] = (k_BT)^{-1}(\mu - V_{ext,y}) - 2DL\int_{z-L/2}^{z+L/2} dz_1 \rho_z(x,z_1) - 2DL\int_{x-L/2}^{x+L/2} dx_1 \rho_x(x_1,z), \quad (5)$$

and

$$\ln[\Lambda^3\rho_z(x,z)] = (k_BT)^{-1}(\mu - V_{ext,z}(x,z)) - 2DL\int_{z-L/2}^{z+L/2} dz_1 \rho_y(x,z_1) - 2D\int_{x-L/2}^{x+L/2} dx_1 \int_{z-L/2}^{z+L/2} dz_1 \rho_x(x_1,z_1), \quad (6)$$

which allow for a straightforward iterative numerical computation on a 2D (x,z) grid. We note that the meaning of the terms on the right side of Eqs. (4)–(6) can easily be inferred from considering the various orientations of the rods (see Fig. 1). It is convenient to introduce the variable $\mu^\star=\mu - k_BT\ln(\Lambda^3/L^2D)$. In the following sections numerical data are given in terms of $\mu^\star$, and we drop the star in order to avoid a clumsy notation.

The bulk phase behavior of this model was studied a long time ago by Zwanzig [11], who found a first-order-isotropic–nematic phase transition similar to Onsager's result for freely rotating rods [15]. Recently, the Zwanzig model has been used to investigate the phase behavior of monodisperse [12,13] and binary [14] rod fluids near a single planar hard wall and confined in slit pore. These calculations yield a wall-induced continuous surface transition from uniaxial to biaxial symmetry. Complete wetting of the wall–isotropic liquid interface by a biaxial nematic film has been found. For the fluids confined by two parallel hard walls, at large slit widths a first-order capillary nematization transition occurs, which terminates in a capillary critical point upon decreasing the slit width.

III. HARD-ROD FLUID NEAR A RIGHT-ANGLED WEDGE AND EDGE

Before studying the hard-rod fluid near the geometrically structured surface shown in Fig. 1 it is instructive to analyze first the fluid around an individual right-angled wedge or edge (see Fig. 2). These simple geometrical structures constitute the building blocks of the structured surface displayed in Fig. 1. An analysis of the size dependence leads to the following decomposition of the grand canonical potential functional of the fluid, which in its bulk is taken to be in the isotropic phase

$$\Omega[\rho(x,z)] = H_y[H_xH_z\omega_b + (H_x+H_z)\gamma_{wI} + \tau_I(\alpha)], \quad (7)$$

where ω_b is the bulk grand canonical potential density, γ_{wI} is the wall–isotropic liquid surface tension at a planar wall, and $\tau_I(\alpha)$ is the line tension of the isotropic liquid with $\alpha=\pi/2$ for the wedge and $\alpha=3\pi/2$ for the edge. The extension H_β of the system in direction $\beta=x,y,z$ is defined as the length available to the rim of the particles at closest approach to the

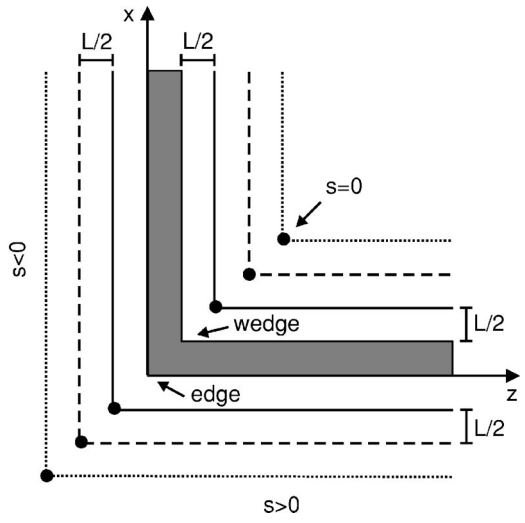

FIG. 2. Cross section of an individual right-angled wedge and edge, respectively. The outer part of the shaded region forms an edge whereas the inner part forms a wedge. The geometrical structures are translationally invariant in the y direction perpendicular to the plane of the figure. In Figs. 4 and 5 density profiles of thin hard rods of length L are shown along the paths indicated by the solid, dashed, and dotted lines, which are parallel to the outer and inner surface, respectively. The paths are parameterized by s such that for each line $s=0$ (•) indicates the position of its corner at $x=z$. $\rho_y(x,z)$ is symmetric around $s=0$ and ρ_x for $s \gtrless 0$ equals ρ_z for $s \lessgtr 0$. Both for the wedge and edge the position of the corner is associated with $(x,z)=(0,0)$; in this figure both cases are superimposed.

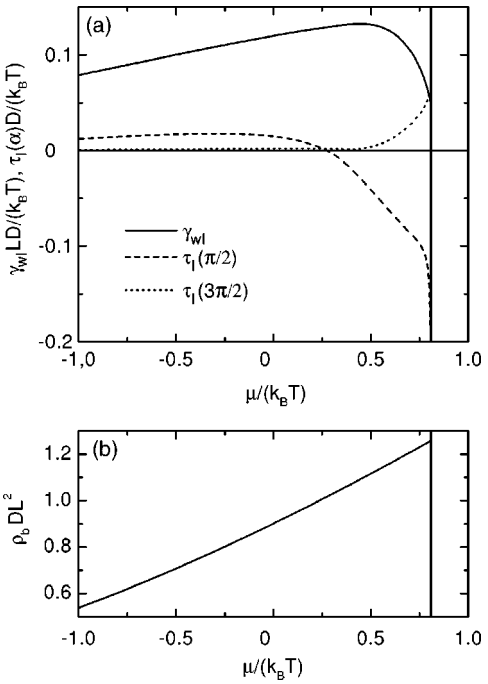

FIG. 3. (a) The wall–isotropic liquid surface tension at a planar wall γ_{wI} (solid line) together with the line tension at a right-angled wedge $\tau_I(\pi/2)$ (dashed line) and edge $\tau_I(3\pi/2)$ (dotted line) of a fluid consisting of thin rods of length L and thickness $D \ll L$ as a function of the chemical potential. The vertical line marks the location of the chemical potential $\mu^{(IN)}/(k_BT)=0.8087227$ at bulk isotropic–nematic coexistence. The wall–isotropic liquid interface is completely wetted by a nematic film, i.e., $\gamma_{wI}=\gamma_{wN}+\gamma_{IN}=0.0498\ k_BT/(LD)$ at $\mu^{(IN)}$, where γ_{wN} is the wall–nematic liquid surface tension and γ_{IN} is the isotropic–nematic interfacial tension [12–14]. At $\mu^{(IN)}$, $\tau_I(3\pi/2)$ is slightly larger than $\gamma_{wI}L$ and $\tau_I(\pi/2)$ attains a finite value that becomes visible only at higher resolutions. $\tau_I(\pi/2)$ changes sign at $\mu/(k_BT)=0.27$. (b) The total particle number density $\rho_b=\rho(x,z\to\infty)$ [see Eq. (8)] of the homogeneous and isotropic bulk fluid as a function of the chemical potential: $\mu/(k_BT)=ln(\rho_b DL^2)-\ln 3+4\rho_b DL^2/3$. At bulk isotropic–nematic coexistence (marked by the vertical line), the density of the isotropic phase is given by $\rho_b DL^2=1.25822486$. This figure allows one to translate values for μ into ρ_b, which is experimentally accessible, and vice versa.

boundary. We restrict our analysis to chemical potentials μ smaller than the chemical potential $\mu^{(IN)}/(k_BT)=0.8087227$ at bulk-isotropic–nematic coexistence. In order to determine the line tensions we first calculate the bulk grand potential density ω_b and the surface tension γ_{wI} by considering a bulk fluid and a fluid near a single hard wall, respectively. Thereafter $\tau_I(\pi/2)$ and $\tau_I(3\pi/2)$ are calculated using the geometry shown in Fig. 2. Figure 3 displays the surface tension γ_{wI} as well as the line tensions $\tau_I(\pi/2)$ and $\tau_I(3\pi/2)$ as a function of the chemical potential. The steric interaction between the particles increases the surface tension with increasing chemical potential. On the other hand, the onset of the surface-induced nematic ordering of the particles leads to a decrease of the surface tension for larger chemical potentials. In the limit of large negative chemical potentials, i.e., for noninteracting particles, the wall–isotropic liquid surface tension as well as the line tensions vanish. The line tension $\tau_I(\pi/2)$ for the fluid near a right-angled wedge exhibits a change of sign with increasing chemical potential while $\tau_I(3\pi/2)>0$ for all values of μ. We note that by construction $\tau_I(\pi)=0$. As a function of α the line tension $\tau_I(\alpha)$ corresponds to the work done per unit length, against the fluid, to change the dihedral angle from π to some value α [16,17]. The corresponding solvation torque is $t_I(\alpha)=-d\tau_I(\alpha)/d\alpha$.

Figures 4 and 5 show the density profiles at the right-angled wedge and edge for a chemical potential $\mu=0$. The profiles are evaluated along lines parallel to the confining walls (see Fig. 2), using a linear parametrization s such that $s=0$ corresponds to the position of the corner. For $s\to\pm\infty$ the density profiles at a planar hard wall are recovered. As is apparent from Fig. 4, the density profile $\rho_y(x,z)$ exhibits a maximum at $s=0$ for the right-angled wedge. This maximum increases upon approaching the corner of the wedge. For a right-angled edge a significant depletion of rods lying parallel to the y axis is found near the corner (see Fig. 5). The sharp features of the density profiles in the presence of the right-angled edge are caused by the vanishing of $\rho_x(x\geqslant -L/2, z\geqslant 0)$ and $\rho_z(x\geqslant 0, z\geqslant -L/2)$, which is due to the presence of the impenetrably hard walls. Such cusps and discontinuities, although less pronounced, have already been found for the density profiles near a planar hard wall using the Zwanzig model [12–14], while the interfacial profiles between demixed fluid phases, as calculated for the same model, exhibit neither cusps nor discontinuities [18]. We do

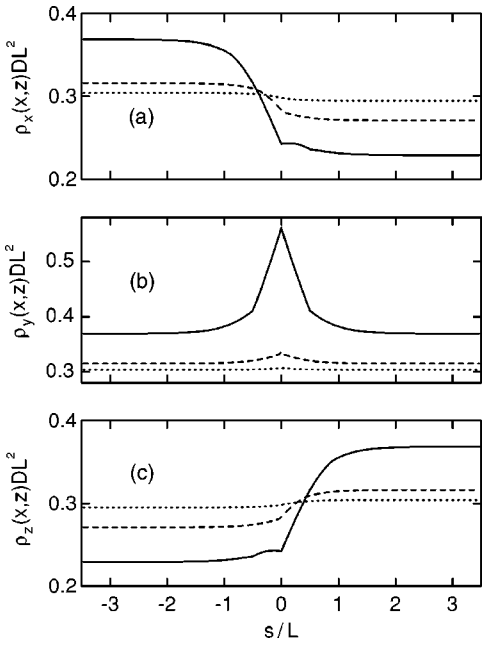

FIG. 4. The density profiles $\rho_x(x,z)$, $\rho_y(x,z)$, and $\rho_z(x,z)$ for thin hard rods of length L thickness $D \ll L$ near a right-angled wedge evaluated along the paths specified in Fig. 2 (using the same line code, i.e., solid, dashed, and dotted lines). The chemical potential is $\mu=0$. The solid curve in (a) [(c)] represents for $s \geqslant 0$ [$s \leqslant 0$] the density profile along the line of closest contact, i.e., rods oriented parallel to the x [z] axis touch the wall with the rim. ρ_y is symmetric around $s=0$ and ρ_x for $s \gtrless 0$ equals ρ_z for $s \lessgtr 0$.

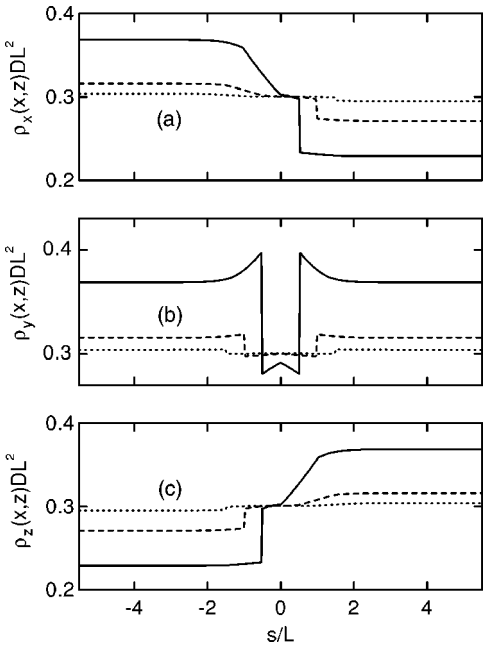

FIG. 5. The density profiles $\rho_x(x,z)$, $\rho_y(x,z)$, and $\rho_z(x,z)$ for thin hard rods of length L and thickness $D \ll L$ near a right-angled edge evaluated along the paths specified in Fig. 2 (using the same line code, i.e., solid, dashed, and dotted lines). The chemical potential is $\mu=0$. The solid curve in (a) [(c)] represents for $s \geqslant L/2$ [$s \leqslant -L/2$] the density profile along the line of closest contact, i.e., rods oriented parallel to the x [z] axis touch the wall with the rim. ρ_y is symmetric around $s=0$ and ρ_x for $s \gtrless 0$ equals ρ_z for $s \lessgtr 0$.

not expect to observe discontinuities in the density profiles for freely rotating rods near an edge, similar to our findings for hard rods near a planar hard wall [19] (see discussion below). Although the calculated density profiles presented in Figs. 4 and 5 can only be considered to be of qualitative significance, we expect that the main features, namely the enrichment [depletion] of rods lying parallel and close to the corner of a wedge [edge] as well as the asymmetry of the density profiles $\rho_x(x,z)$ and $\rho_z(x,z)$ with respect to the line $s=0$, remain valid for freely rotating rods.

In order to understand the structure of the density profiles displayed in Figs. 4 and 5, it is instructive to apply the idea of entropically driven forces (see, e.g., Ref. [20]) to the Zwanzig model. We consider rods of a given orientation along the x, y, and z axes as belonging to one of three "species." Such a three-component fluid maximizes its entropy by maximizing the volume accessible per rod. Although there exist only steric repulsions between pairs of particles, maximizing the entropy in the fluid mixture can lead to an effective entropic attraction between the rods and the walls. Figure 6(b) demonstrates that, when a rod of a given species approaches a planar wall (represented in gray), the total volume *available* to rods of the other species increases. This increases the total entropy of the mixture by an amount proportional to the size of the excluded-volume overlap region (represented in black) multiplied by the pressure. For a rod lying close and parallel to a right-angled wedge [edge] the corresponding excluded-volume overlap region is increased [decreased] (see Figs. 6(c) and 6(d), respectively) leading to an enrichment [depletion] of such rods close to the corner of a wedge [edge]. The results may be interpreted in terms of a repulsive barrier of an effective potential repelling a rod, which is oriented parallel to the corner of an edge, approaching the edge from the side, and practically preventing it from passing around the corner. On the other hand, the effective potential acting on a rod, which is oriented parallel to the corner of a wedge, is "pushing" it into the corner. For a detailed analysis of these mechanisms acting on mixtures of hard spheres near edges and wedges, see Ref. [5] and in particular Figs. 5 and 7 therein.

The simple illustration in Fig. 6(d) is also helpful for understanding the aforementioned discontinuities in the density profiles near the right-angled edge (see Fig. 5). When a thin rod ($D \ll L$), which is oriented parallel to the edge, approaches the edge from the side, the excluded-volume overlap drops abruptly to zero before the rod is passing around the corner. This causes the discontinuities in the density profiles along the paths specified in Fig. 2. For freely rotating rods, the corresponding excluded-volume overlap decreases smoothly to zero because of the huge number of differently oriented rods acting on the rod which is oriented parallel to the edge. It is worthwhile to emphasize that the concept of effective entropic interactions is valid for arbitrary thickness $D \neq 0$ of the rods. However, for very thin rods the excluded volume and the excluded volume overlap region are similar to plane and line segments. For $D=0$ the excluded volume vanishes as expected on physical grounds.

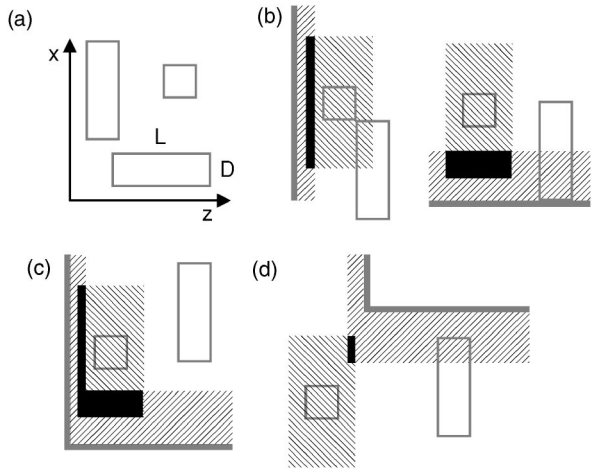

FIG. 6. Illustrations of the effective entropic interactions of hard rods with surfaces. (a) Schematic side view of rectangular rods of length L and thickness D with orientations along the x, y, and z axes, where the y axis is perpendicular to the plane of the figure. (b) Due to the steric interaction, the centers of mass of rods with x direction are excluded from the hatched regions surrounding the rods with y direction (quadratic cross-section) and the walls (thick gray lines). Here one rod with x direction touches a rod with y direction (left) while another rod with x direction fully touches the wall which is oriented parallel to the z axis (right). The rods with x direction are viewed as depletion agents leading to an effective interaction between the rod with y direction and the walls. When rods with orientations along the y axis are sufficiently separated from each other and from the walls, the volume accessible to the rods with x direction is the total volume of the container minus the volume of the hatched regions. However, when a rod oriented parallel to the y axis is close to a wall, the volume accessible to the rods with x direction increases by the excluded-volume overlap region marked in black. The corresponding increase in entropy induces an effective attractive force between rods with an orientation parallel to the y axis and the wall. (c) In a corner of a right-angled wedge (thick gray lines), the overlap volume (black region) is larger than the one on a flat wall leading to an enrichment of rods lying parallel and close to the corner of the wedge [see Fig. 4(b)]. (d) Close to a right-angled edge (thick gray lines), the overlap volume is smaller than the one on a planar wall. Therefore the density of rods lying parallel and close to the edge is smaller than the density near a planar hard wall at the same chemical potential [see Fig. 5(b)]. Similar considerations hold for the rods with z direction acting as depletion agents on the rod with y direction. The rods with y direction are exposed to the superposition of both effective interactions. For thin rods ($0<D\ll L$) the excluded volumes are similar to plane and line segments.

Finally, we briefly discuss the phase behavior of hard rods confined in a hard pore of square cross section. The immediate consequence of the pore is that rods oriented perpendicular to the confining walls cannot approach closer than a center-of-mass distance $L/2$. There is a pronounced increase of the density of rods orientated parallel to the main axis of the pore in the corners of the pore because of the aforementioned effective entropic attraction. For sufficiently large cross sections of the pore, we observe coexistence between an isotropic phase and a capillary-condensed nematic phase. The density profile of the capillary-condensed nematic phase is characterized by a nematic phase throughout the pore, whereas the density profile of the coexisting phase decays toward an isotropic phase in the middle of the pore. For small pore cross sections, a sharp capillary nematization transition no longer occurs and is replaced by a steep but continuous filling upon increasing the chemical potential. For the same fluid confined in a slit pore the confinement effects are weaker. Thus, in the slit pore we observe capillary nematization at a higher chemical potential corresponding to a higher particle number density of the bulk fluid. However, the spatially averaged particle number density of the coexisting inhomogeneous isotropic phase in the slit pore is smaller than the corresponding one in the pore of square cross section.

IV. HARD-ROD FLUID IN CONTACT WITH A PERIODICALLY STRUCTURED HARD WALL

We now turn our attention to the properties of the hard-rod fluid in contact with the hard wall shown in Fig. 1. The surface of the wall is periodically patterned with rectangular hard barriers of width w and height h, where the periodicity is denoted by p. We focus on the numerically determined orientationally averaged number density profile

$$\rho(x,z) = \rho_x(x,z) + \rho_y(x,z) + \rho_z(x,z) \tag{8}$$

and the excess adsorption Γ defined as

$$\Gamma = \int dx\, dz[\rho(x,z) - \rho_b], \tag{9}$$

where $\rho_b = \rho(x, z \to \infty)$ is the total particle number density of the homogeneous bulk fluid. The volume $V = \int dx\, dy\, dz$ of the system is defined as the total volume of the container, i.e., the left boundary of the system displayed in Fig. 1 is taken to be the surface $z_s(x)$ of the substrate wall, which implies that the trenches between the barriers contribute to V. Figure 7 displays Γ for various values of the barrier height h and two values of the barrier width w at a fixed periodicity p of the surface pattern. For noninteracting rods ($\mu \to -\infty$), the calculated excess adsorption reveals a slight depletion close to the surface ($\Gamma < 0$) because there is less space available to the rods in the presence of the impenetrably hard walls. For the same reason this depletion becomes more pronounced with increasing height of the barriers (i.e., increasing the actual exposed solid area). Upon increasing the chemical potential, the excess adsorption increases and exhibits a change of sign because of the aforementioned entropic attraction between the rods and the surface [see Fig. 6]. For small barrier heights, Γ increases smoothly upon increasing the chemical potential, while a pronounced variation of the excess adsorption is found for large barrier heights at a chemical potential smaller than the chemical potential $\mu^{(IN)}$ at bulk isotropic–nematic coexistence. Moreover, the calculation renders Γ to diverge logarithmically as $\mu \to \mu^{(IN)}$. Near $\mu^{(IN)}$ the excess adsorption can be fitted by $\Gamma = A_1 - A_2 \ln[(\mu^{(IN)} - \mu)/(k_B T)]$, with fit parameters A_1 and A_2, where $A_2 > 0$ turns out to be independent of the surface pattern. The logarithmic diver-

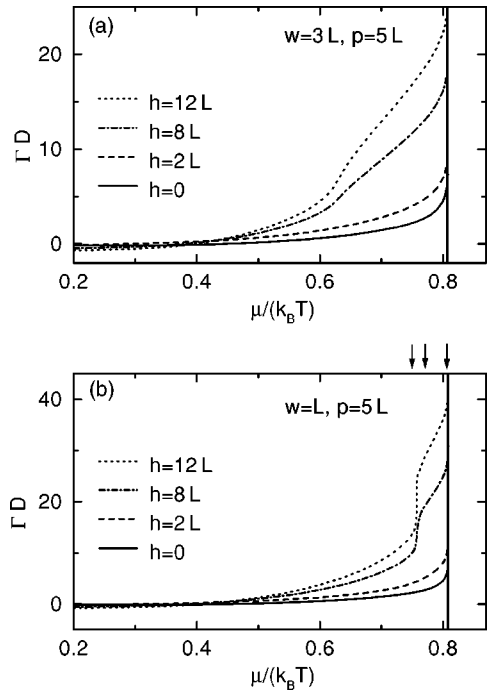

FIG. 7. The excess adsorption Γ [see Eq. (9)] of a fluid consisting of thin hard rods of length L and thickness $D \ll L$ near a geometrically structured wall as shown in Fig. 1 for various barrier heights: $h=0$ (solid curves); $h=2\ L$ (dashed curves); $h=8\ L$ (dash-dotted curves); $h=12\ L$ (dotted curves). The periodicity is $p=5\ L$ and the barrier width is $w=3\ L$ in (a) and $w=L$ in (b). The vertical lines mark the value of the chemical potential $\mu^{(IN)}/(k_BT) = 0.8087227$ at bulk isotropic–nematic coexistence. In all cases Γ diverges logarithmically as $\mu \to \mu^{(IN)}$. Figure 8 exhibits density profiles for the system with $h=8\ L$ in (b) for the three chemical potentials $\mu=0.75$, 0.77, 0.808 k_BT marked by arrows. The chemical potential $\mu \simeq 0.757\ k_BT$ corresponding to the pronounced variation (no jump but steep increase) of Γ for $h=12\ L$ in (b) turns out to agree with the chemical potential at the occurrence of the first-order capillary nematization transition of the same fluid confined in a corresponding slit pore of width $p-w=4\ L$. Neither the curves in (a) nor in (b) intersect at a single point.

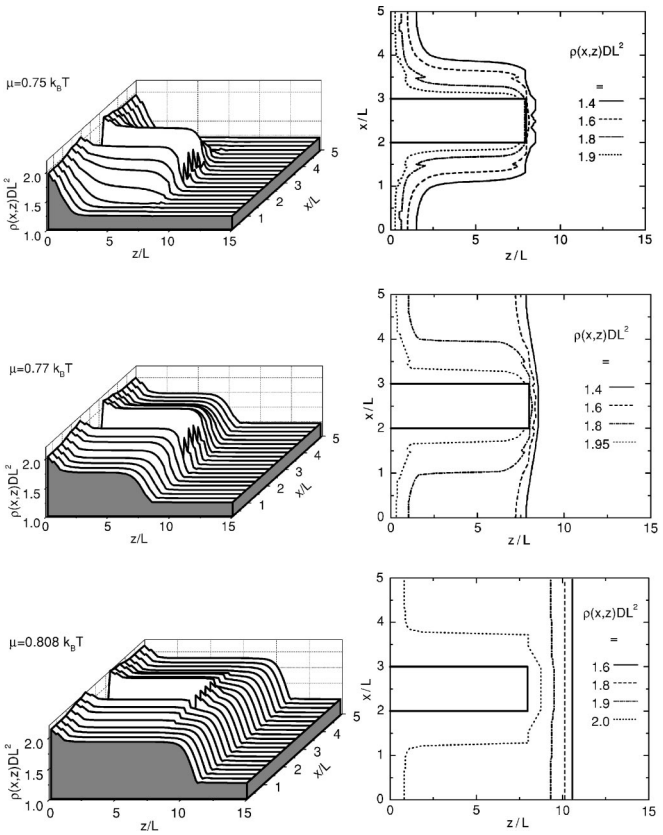

FIG. 8. Orientationally averaged total density profile $\rho(x,z)$ [see Eq. (8)] of thin rods of length L and thickness $D \ll L$ in contact with a hard wall for three chemical potentials $\mu=0.75$, 0.77, 0.808 k_BT, where $\mu^{(IN)}/(k_BT)=0.8087227$ is the chemical potential at bulk isotropic–nematic coexistence. The corresponding contour plots are shown on the right. The sharp structures in the contour lines are caused by the discreteness of the orientational degrees of freedom. The wall at $z=0$ is patterned with rectangular (parallel) barriers of width $w=L$ with $x_0=2.5\ L$, height $h=8\ L$, and periodicity $p=5\ L$ (see Fig. 1). The corresponding excess adsorption is represented by the dash-dotted line in Fig. 7(b), and the three chemical potentials are marked by arrows in Fig. 7(b). For $\mu=0.808\ k_BT$ the interface between the higher-density nematic film on the wall and the lower-density isotropic bulk fluid ($z \to \infty$) resembles closely the interface between the free isotropic–nematic interface between coexisting bulk phases, with coexisting densities $\rho_b^{(I)}DL^2=1.25822486$ and $\rho_b^{(N)}DL^2=1.91544377$. At $\mu \simeq 0.757\ k_BT$ the trenches undergo a nematization filling, which is a smooth but steep variation of the density distribution.

gence of Γ is consistent with complete wetting of the wall–isotropic fluid interface by a nematic film in the absence of algebraically interaction potentials [21]. A similar behavior of the excess adsorption close to $\mu^{(IN)}$ has been found for the same fluid near a planar hard wall [12–14].

To understand the origin of the calculated excess adsorptions, it is instructive to study the variation of the density profiles with increasing chemical potential. The orientationally averaged density profiles $\rho(x,z)$ shown in Fig. 8 demonstrate that the wetting of the nonplanar wall–isotropic liquid interface by a higher-density nematic film occurs as a two-stage process where first the nematic phase fills the space between the barriers until an almost planar isotropic–nematic liquid interface has formed separating the higher-density nematic fluid in the space between the barriers from the lower-density isotropic bulk fluid. In the second stage a nematic film of diverging film thickness develops upon approaching the chemical potential at bulk isotropic–nematic coexistence. In the presence of the patterned wall, the director (the average orientation of the rods) of the nematic phase is parallel to the y axis because of the aforementioned effective entropic attraction between rods oriented parallel to the right-angled wedges of the barriers [see Fig. 6(c)]. Upon approaching the chemical potential at bulk isotropic–nematic coexistence, i.e., $\mu > 0.757\ k_BT$ in Fig. 7 (with this value of the kink position being largely independent of h), the calculated density profiles at the isotropic–nematic interface become virtually indistinguishable from the free isotropic–nematic interface between coexisting bulk phases, as expected for the case of complete wetting. In this limit this

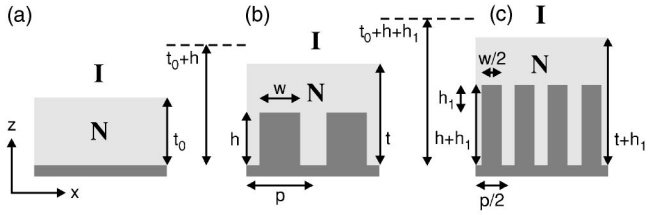

FIG. 9. Schematic side view of a planar wall and two geometrically patterned walls (dark gray regions). The y direction is perpendicular to the plane of the figure (see Fig. 1). (a) The planar wall–isotropic (I) liquid interface is wetted by a nematic (N) film of thickness t_0. (b) At the same chemical potential the film thickness t on the geometrically patterned wall is larger than h and smaller than t_0+h, where $t=t_0+h$ for $w=p$. (c) Illustration of Eqs. (10) and (11); w and p are half as large as in (b) and h is increased by h_1.

holds irrespective of the actual values of the width w, height h, and periodicity p. However, the thickness of the emerging nematic film depends on the aforementioned model parameters and the chemical potential.

A very *thin* nematic liquid layer–corresponding to a large undersaturation–follows the substrate pattern, whereas a sufficiently thick layer is essentially flat (see Fig. 8). In the following, we will be exclusively concerned with *thick* nematic films, allowing us to define an x-independent film thickness $t=L\times f((h/L),(p/L),(w/L),(\mu/k_BT))$ defined as the distance z_m between the midpoint of the density profile for the planar isotropic–nematic interface and the substrate surface $z=0$; f is a scaling function appearing on the basis of dimensional analysis. The minimal film thickness for which a planar isotropic–nematic liquid interface is still possible is $t\gtrsim h$. We consider the situation as illustrated in Fig. 9(a), where for a given chemical potential μ a nematic (N) film of thickness t_0 intrudes between a planar hard wall and an isotropic (I) bulk fluid. At the same chemical potential the film thickness t of the fluid in contact with a geometrically patterned wall is larger than the height of the barriers h and smaller than t_0+h [see Fig. 9(b)]. For $p=w$ it follows that $t=t_0+h$ as expected on physical grounds. It is worthwhile to mention that $f[(h/L),(p/L),(w/L),(\mu/k_BT)]$ as function of w/L for given h/L, p/L, and $\mu/(k_BT)$ exhibits a discontinuity upon approaching $w\to 0$ because the ratio of the actual substrate area (including the side planes of the rectangular blocks) per period p over the one projected onto the $x-y$ plane drops abruptly from $(p+2h)/p$ to 1 for $w\equiv 0$. Hence, due to geometric constraints the film thickness in the presence of infinitely thin barriers differs from the one in the absence of the barriers. Moreover, we find the following properties, which are schematically visualized in Figs. 9(b) and 9(c)

$$t=L\times f\left(\frac{h}{L},\frac{p}{L},\frac{w}{L},\frac{\mu}{k_BT}\right)=L\times g\left(\frac{h}{L},\frac{w}{p},\frac{\mu}{k_BT}\right) \qquad (10)$$

and for fixed w/p and $\mu/(k_BT)$

$$t(h+h_1)=h_1+t(h),\quad h\gtrsim L. \qquad (11)$$

Equation (10) states that upon varying the barrier width w and the periodicity p such that the ratio $(p-w)/w$ of the substrate area at the bottom $z=0$ over the substrate area at the top $z=h$ is kept fixed, the film thickness does not change for a given barrier height h, chemical potential μ, and L. This result is reminiscent of the Cassie equation [22]. Cassie considered a simple liquid in contact with a smooth, but chemically striped surface with periodicity p such that on stripes of width w one has a contact angle ϑ_1 and in between ϑ_2. The apparent average contact angle is given by

$$\cos\,\vartheta_{app}=\frac{w}{p}\cos\,\vartheta_1+\left(1-\frac{w}{p}\right)\cos\,\vartheta_2. \qquad (12)$$

Since ϑ_{app}, ϑ_1, and ϑ_2 are determined uniquely by t_{app}, t_1, and t_2 via the corresponding effective interface potentials [see Eq. (4.56) in Ref. [21]], Eq. (12) states that the apparent film thickness t_{app} depends only on the ratio w/p, which is the analogue of Eq. (10). Whereas Eq. (10) is valid for all values of w/L, h/L, and p/L, for molecular-scale surface patterns with barrier heights $h\lesssim L$ we find deviations from Eq. (11).

The wetting of the nonplanar wall–isotropic liquid interface by a nematic film is driven by the steric interaction of the rods with the solid substrate, which is mediated by the fluid occupying the space between the barriers. As the barrier height h increases the interaction between rods located at $z>h$, and the part of wall which is located at $z=0$ weakens, such that for large height h and small width w, wetting is dominated by the interaction with the *fluid* in the space between the barriers and not by that with the *solid* substrate at $z=0$. However, one has to take into account that the rods in the trenches between the barriers interact not only with the part of the substrate wall, which is located at $z=0$, but also with the side planes of the rectangular blocks which are parallel to the $z-y$ plane.

V. SUMMARY

We have studied hard-rod fluids near geometrically structured walls using Zwanzig's model of square parallelepipeds with only three allowed orientations (Fig. 1). Within the framework of a density functional theory, the grand potential functional is minimized numerically and density profiles, excess adsorptions, as well as surface and line tensions are determined leading to the following main results:

(i) The line tension for the isotropic fluid in contact with a right-angled wedge (see Fig. 2) exhibits a change of sign with increasing chemical potential, while the line tension for the fluid in contact with a right-angled edge as well as the wall–isotropic fluid surface tension at a planar hard wall are positive (Fig. 3).

(ii) Figures 4 and 5 demonstrate an enrichment [depletion] of rods lying parallel and close to the corner of a right-angled wedge [edge]. On the basis of effective entropic forces between the rods and the walls (see Fig. 6), the results may be interpreted in terms of a repulsive barrier of an effective potential repelling a rod, which is oriented parallel to

the corner of an edge, and approaches the edge sidewise, and practically preventing it from passing around the corner. The effective potential acting on a rod that is oriented parallel to the corner of a wedge is larger than the one close to a planar wall. Building on the effects demonstrated in Figs. 4–6, it seems possible to devise structures that create localized and directional entropic force fields for both natural and synthetic rodlike colloids.

(iii) Coexistence between an isotropic and a capillary condensed nematic phase is observed for the fluid confined in a hard pore of square cross section, provided the cross section is sufficiently large. The density profile of the capillary-condensed nematic phase is characterized by a nematic phase throughout the pore, whereas the density profile of the coexisting phase decays towards an isotropic phase in the middle of the pore. For the same fluid confined in a slit pore the confinement effects are weaker, i.e., in the slit pore one observes capillary nematization only at a higher chemical potential.

(iv) From the calculated excess adsorptions (Fig. 7) and density profiles (Fig. 8) of a fluid consisting of hard rods near the geometrically structured wall shown in Fig. 1, we conclude that complete wetting of the nonplanar wall–isotropic liquid interface by a nematic film occurs as a two-stage process. In the first stage the nematic phase fills the space between the barriers until an almost planar isotropic–nematic liquid interface has formed, separating the higher-density nematic fluid in the trenches between the barriers from the lower-density isotropic bulk fluid. In the second stage, a nematic film of diverging film thickness develops upon approaching the chemical potential at bulk isotropic–nematic coexistence. The film thickness, defined as the distance between the midpoint of the density profile for the almost planar isotropic–nematic interface and the substrate bottom at $z=0$, is larger for the fluid near the geometrically structured wall than the one for the fluid near a planar wall at the same chemical potential (Fig. 9).

Finally, we note that phenomena which emerge from the contact of a rod fluid which is in its bulk in the nematic phase are also interesting because of the possibility to deliver external lateral structures deep into the bulk of the adjacent fluid which offers a convenient means to image patterned surfaces. Applying a fundamental measure theory to the system under consideration will allow one to study thick rods or platelets [23] as well as rods with continuously varying orientations [24] near patterned surfaces.

[1] A. D. Dinsmore, A. G. Yodh, and D. J. Pine, Nature (London) **383**, 239 (1996).
[2] Y. Yin and Y. Xia, Adv. Funct. Mater. **14**, 605 (2002).
[3] M. Kinoshita and T. Oguni, Chem. Phys. Lett. **351**, 79 (2002).
[4] M. Kinoshita, J. Chem. Phys. **116**, 3493 (2002).
[5] P. Bryk, R. Roth, M. Schoen, and S. Dietrich, Europhys. Lett. **63**, 233 (2003).
[6] R. Castaneda-Priego, A. Rodriguez-Lopez, and J. M. Mendez-Alcaraz, J. Phys.: Condens. Matter **15**, 3393 (2003).
[7] M. Schoen and S. Dietrich, Phys. Rev. E **56**, 499 (1997).
[8] D. Boda, K.-Y. Chan, D. Henderson, D. T. Wasan, and A. D. Nikolov, Langmuir **15**, 4311 (1999).
[9] D. J. Diestler and M. Schoen, Phys. Rev. E **62**, 6615 (2000).
[10] M. Schoen, Colloids Surf., A **206**, 253 (2002).
[11] R. Zwanzig, J. Chem. Phys. **39**, 1714 (1963).
[12] R. van Roij, M. Dijkstra, and R. Evans, Europhys. Lett. **49**, 350 (2000).
[13] R. van Roij, M. Dijkstra, and R. Evans, J. Chem. Phys. **113**, 7689 (2000).
[14] L. Harnau and S. Dietrich, Phys. Rev. E **66**, 051702 (2002).
[15] L. Onsager, Phys. Rev. **62**, 558 (1942); L. Onsager, Ann. N.Y. Acad. Sci. **51**, 627 (1949).
[16] J. R. Henderson, Physica A **305**, 381 (2002).
[17] J. R. Henderson, J. Chem. Phys. **120**, 1535 (2004).
[18] M. Bier, L. Harnau, and S. Dietrich, Phys. Rev. E **69**, 021506 (2004).
[19] L. Harnau and S. Dietrich, Phys. Rev. E **65**, 021505 (2002).
[20] R. Roth, R. Evans, and S. Dietrich, Phys. Rev. E **62**, 5360 (2000).
[21] S. Dietrich, in *Phase Transitions and Critical Phenomena*, edited by C. Domb and J. L. Lebowitz (Academic, London, 1988), Vol. 12, p. 1.
[22] A. B. D. Cassie, Discuss. Faraday Soc. **3**, 11 (1948).
[23] L. Harnau, D. Rowan, and J.-P. Hansen, J. Chem. Phys. **117**, 11359 (2002).
[24] M. Schmidt, Phys. Rev. E **63**, 050201 (2001).